Anal Bioanal Chem (2009) 393:1143–1149
DOI 10.1007/s00216-008-2418-9

ORIGINAL PAPER

Experimental and theoretical studies of the optimisation of fluorescence from near-infrared dye-doped silica nanoparticles

Robert I. Nooney · Ciara M. N. McCahey · Ondrej Stranik · Xavier Le Guevel · Colette McDonagh · Brian D. MacCraith

Received: 15 August 2008 / Revised: 16 September 2008 / Accepted: 17 September 2008 / Published online: 10 October 2008

Abstract There is substantial interest in the development of near-infrared dye-doped nanoparticles (NPs) for a range of applications including immunocytochemistry, immunosorbent assays, flow cytometry, and DNA/protein microarray analysis. The main motivation for this work is the significant increase in NP fluorescence that may be obtained compared with a single dye label, for example Cy5. Dye-doped NPs were synthesised and a reduction in fluorescence as a function of dye concentration was correlated with the occurrence of homo-Förster resonance energy transfer (HFRET) in the NP. Using standard analytical expressions describing HFRET, we modelled the fluorescence of NPs as a function of dye loading. The results confirmed the occurrence of HFRET which arises from the small Stokes shift of near-infrared dyes and provided a simple method for predicting the optimum dye loading in NPs for maximum fluorescence. We used the inverse micelle method to prepare monodispersed silica NPs. The NPs were characterised using dynamic light scattering, UV spectroscopy, and transmission electron microscopy (TEM). The quantum efficiency of the dye inside the NPs, as a function of dye loading, was also determined. The fluorescent NPs were measured to be approximately 165 times brighter than the free dye, at an optimal loading of 2% (*w*/*w*). These experimental results were in good agreement with model predictions.

R. I. Nooney · C. M. N. McCahey · O. Stranik · X. Le Guevel · C. McDonagh · B. D. MacCraith (✉)
Biomedical Diagnostics Institute,
National Centre for Sensor Research,
School of Physical Sciences, Dublin City University,
Glasnevin, Dublin 9, Ireland
e-mail: Brian.Maccraith@dcu.ie

Keywords Fluorescence · Nanoparticles · Energy transfer · Biosensing

Introduction

Due to their high sensitivity, fluorescence-based bioassays are widely used in biomedical diagnostics. The most commonly used fluorescent labels are organic or inorganic molecules containing π-conjugated ring structures [1]. A large number of commercial dyes with absorption bands across the visible and near-infrared (NIR) spectrum are used routinely for optical bioassays.

While fluorescence-based detection offers high sensitivity in general, there is often a low level of detectable fluorescence from the bioassay platform due to the relatively low surface coverage of labelled biomolecules. Hence, there is a need for brighter fluorescent labels which will increase sensitivity and lower the limit of detection (LOD) in optical bioassays, particularly for low-volume samples. To meet this need, there has been a great deal of work on the development of second-generation labels, such as quantum dots, dye-doped silica nanoparticles (NPs), and polystyrene beads. These labels have been shown to increase signal to noise ratios, sensitivity, and LOD in biosensing applications [2–5].

In this work we report on the synthesis of NIR dye-doped silica NPs and the optimization of fluorescence for application as a second-generation label. Silica matrices provide a stable environment which is resistant to both chemical attack and mechanical stress. Silica surfaces can also be easily functionalised with bioreactive groups using conventional organosilane chemistry [2]. There are two

principal methods for the preparation of monodispersed silica NPs—the Stöber method and the inverse micelle method. The Stöber method uses an ammonium hydroxide catalyst in ethanol and water to control the hydrolysis and condensation rates of alkoxysilanes [6]. Recently, a modification of the Stöber method was developed at Cornell University, whereby monodispersed dye-doped silica NPs were synthesised down to 15 nm in diameter [7]. These NPs, called C-dots have fluorescence levels approaching those of quantum dots and, for certain dyes, the rate of photobleaching is reduced by an order of magnitude. In the case of the inverse micelle method, NPs are synthesised inside surfactant-stabilised water droplets which are dispersed in a non-polar solvent [8]. This method is attractive because it is relatively easy to reproducibly prepare monodispersed NPs in diameters from several microns down to 15 nm, and it is the method employed in this work. The NP diameter is dependent on the concentration of catalyst, water, alkoxysilane, and type of surfactant used. These NPs can accommodate high dye loadings (up to 20% *w*/*w*), are significantly more fluorescent than the free dye and also exhibit less photobleaching than the free dye [9]. Fluorescent NPs have been used previously for immunoassays, immunocytochemistry, and DNA/protein microarray analysis [10, 11]. In other work, silica NPs have been doped with multiple fluorescent dyes to achieve Förster resonance energy transfer (FRET) [12]. Using only a single excitation wavelength multiple emission signatures with large Stokes shifts were obtained. These NPs have been used in multiplexed imaging of pathogenic bacteria, where individual fluorescent signatures were obtained for each species [13].

NIR dyes offer several advantages over other organic dyes that fluoresce at shorter wavelengths, for example fluorescein or rhodamine red. In common with other work on organic dyes, we classify a NIR dye as a dye having a fluorescence excitation maximum greater than 650 nm [14]. At NIR wavelengths there is low background interference from the fluorescence of biological molecules, solvents, and substrates. Furthermore, whole blood has very weak absorption in the NIR region, thus reducing the need for whole-blood filtering for assays using whole blood. NIR light can also penetrate skin and tissue to several millimetres, enabling fluorescence detection in dermatological or in-vivo diagnostic devices.

The main focus of this paper is the synthesis and characterisation of silica NPs which are doped with a relatively inexpensive NIR-dye, as a surrogate for the widely used cyanine dyes in this spectral region, and which exhibit more than two orders of magnitude increase in fluorescence intensity compared with a single dye molecule. The work highlights the particular issues associated with the use of NIR dyes in NPs and points to strategies for further improvements. In particular, the paper addresses the problem of homo-Förster resonance energy transfer (HFRET) arising from the small Stokes shift of the dye and identifies the optimum dye loading which yields maximum fluorescence.

Theoretical background

The dye used in this work is 4,5-benzo-1′-ethyl-3,3,3′,3′-tetramethyl-1-(4-sulfobutyl)indodicarbocyanin-5′-acetic acid *N*-succinimidyl ester, more commonly referred to as NIR-664-N-succinimidyl ester (purchased from Sigma-Aldrich). At the high pHs required for synthesis of silica NPs, the NIR-664-N-succinimidyl ester dye was significantly more stable than commonly used NIR dyes such as Cy5, Alexa Four 670, and squaraines. Moreover, NIR-664-N-succinimidyl ester is significantly cheaper than most other commercially available NIR dyes used in biological sensing. This dye has a quantum efficiency of 23%, a molar absorptivity of 187,000 L mol^{-1} cm^{-1} and fluorescence excitation and emission wavelengths of 672 nm and 694 nm, respectively, in isopropanol [15] (Fig. 1).

In the case of weak excitation, the fluorescence of a single dye molecule is proportional to the absorption cross-section of the molecule, the intensity of the excitation beam, and the quantum efficiency, φ, of the molecule [16]. However, the fluorescence is changed when in close proximity to a second molecule. This effect can be described using Förster resonance energy transfer (FRET). FRET is commonly used in molecular biology for quantifying protein-protein interactions or conformational changes. For the special case where FRET occurs between two identical molecules, the effect is called homo-FRET (HFRET). This effect is commonly observed for fluorescent molecules which have a small Stokes shift, which is the case for many NIR dyes. HFRET is the process whereby

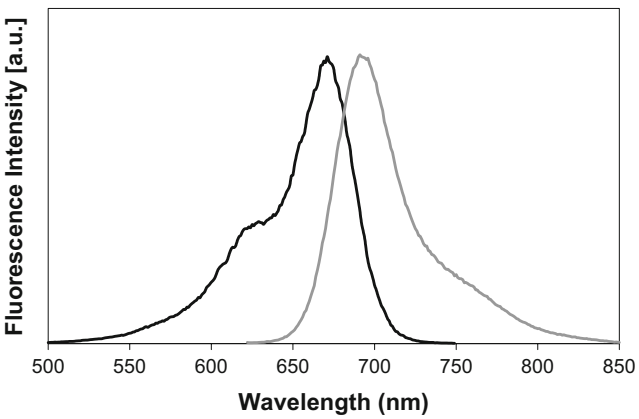

Fig. 1 Excitation and emission fluorescence spectra of pure NIR-664-*N*-succinimidyl ester in isopropanol

part of this energy is transferred from an excited molecule, called the donor, to another dye molecule in its ground state, called the acceptor.

Under the above conditions the emitted fluorescence F_o* from the donor molecule is reduced in the following way:

$$F_0^* = F_0(1 - E_f) \quad E_f = \frac{1}{1 + (r/R_0)^6}$$

where, F_o is the unmodified fluorescence of the donor molecule. The term E_f is called the efficiency of FRET and is highly dependent on the distance between donor and acceptor, r, where R_o is the Förster radius. The Förster radius is the distance between donor and acceptor at which the efficiency of FRET is 50% [17]. For NIR-664-succinimidyl ester dye trapped inside a silica matrix with a refractive index of 1.5, we calculated a Förster radius of 5.35 nm using standard equations [17].

After energy transfer to the acceptor molecule, the transfer energy (F_0E_f) can be re-emitted or HFRET-transferred back to the first molecule. The re-emitted energy is given by $F_o\varphi E_f(1 - E_f)$. This transfer of energy between the two molecules is repeated and the total amount of emitted fluorescence, F_T, can be expressed as follows:

$$F_T = \sum_{i=0}^{\infty} F_0 \phi^i E_f^i (1 - E_f) = F_0 \frac{1 - E_f}{1 - \phi E_f}$$

Using the above equations, one can derive the following expression for the total fluorescence, $F_{T,n}$, from the excitation of multiple fluorophores inside a silica NP:

$$\frac{F_{T,n}}{F_0} = n \frac{1 - E_f}{1 - \phi E_f}$$

where n is the number of fluorophores inside the silica NP. The brightness ratio $F_{T,n}/F_o$ is a measure of the fluorescence of a single NP divided by the fluorescence of one dye molecule. In this model, we assume the dye molecules are evenly distributed in the NP and HFRET is only counted for nearest-neighbour molecules. In addition, this model does not account for complex aggregation of the dye, such as dimerization, or changes in the quantum efficiency of the dye due to encapsulation in the NP.

We calculated the brightness ratio for multiple fluorophores in spherical NPs of different sizes as a function of the NPs radius and the number of molecules (Fig. 2) As would be expected, the brightness ratio increases with particle size. The ratio also increases with the number of dye molecules at very low dye loadings. However, as the number of dye molecules increases, and consequently as their intermolecular separation decreases, the brightness ratio decreases significantly. The maximum brightness ratio for a particle with a radius of 28 nm was found to be 342, with a dye loading of 682 molecules or 0.37% (*w*/*w*). At this value, the dye molecules are approximately 5.1 nm apart, which is slightly shorter than the Förster radius, at 5.35 nm. Even at such a low loading of dye molecules there is not enough distance between the dye molecules to prevent a significant drop in fluorescence. The theoretical predictions of maximum brightness ratio are compared with experimental values later in the paper.

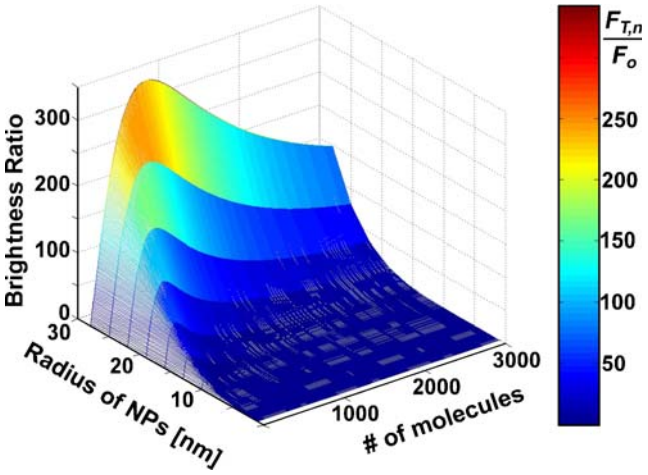

Fig. 2 The change in brightness ratio of dye molecules as a function of the number of dye molecules inside the NP and the radius of the NP modelled using HFRET

Experimental

Materials

Triton X-100 (Union Carbide), *n*-hexanol (anhydrous, >99%), cyclohexane (anhydrous 99.5%), ammonium hydroxide (28% in H_2O >99.99%), tetraethylorthosilica (TEOS, 99.99%), aminopropyltrimethoxysilane (APTMS, 97%), aminopropyltriethoxysilane (APTES, 99%), 3-(trihydroxysilyl)propyl methyl phosphonate, monosodium salt solution (THPMP, 42% (*w*/*w*) in water), triethylamine (>99%), and absolute ethanol were all purchased from Sigma-Aldrich Ireland and used without further purification. Deionised water (<18 MΩ) was obtained from a Milli-Q system from Millipore Ireland.

Synthesis of NPs

First, 15.6 mg NIR-664-*N*-succinimidyl ester was dissolved in 5 mL anhydrous *n*-hexanol. To this solution, 5.021 μL pure APTES and 3 μL triethylamine were added. The mixture was agitated for 24 h to ensure conjugation of the NIR dye to the organosilane. We prepared NPs containing 0.25, 0.5, 1, 2, 3, 6, and 10% (*w*/*w*) NIR-664-succinimidyl ester using the microemulsion method [18]. The procedure for preparing 2% (*w*/*w*) NP is detailed below. NPs with

other concentrations were prepared in a similar way. Briefly, the microemulsion was formed by mixing cyclohexane oil phase (15 mL), *n*-hexanol co-solvent (3.256 mL), and Triton X-100 surfactant (3.788 g) in 30-mL plastic bottles. To form the microemulsion, 0.96 mL deionised water was added and the solution stirred for 5 min. Following this, 0.2 mL TEOS and 0.16 mL NH_4OH were added to start the growth of the silica NPs. After 30 min, 0.344 mL the NIR-664-APTES conjugate was added. The reaction was stirred for 24 h, after which 0.1 mL TEOS was added with rapid stirring.

After 30 min, 0.08 mL of the organosilane, 3-(trihydroxysilyl)propyl methyl phosphonate, monosodium salt solution (THPMP), (42% (*w*/*w*) in water) was added with stirring to prevent aggregation of the nanoparticles [19]. After a further 5 min, 0.02 mL bioreactive organosilane, aminopropyltrimethoxysilane (APTMS), was added to and the solution stirred for a further 24 h. The APTMS has a free primary amine group for crosslinking to biomolecules. The NPs were separated from the solution with the addition of excess absolute ethanol and centrifuged twice with ethanol and once with deionised water. Sonication was used between the washing steps to resuspend the NPs. The NPs were dispersed in deionised water, at 2.0 mg mL^{-1} and stored in the dark at 4 °C.

Instrumentation

UV-visible extinction spectra of colloidal suspensions of NPs were measured using a Cary 50 scan UV-visible spectrophotometer (Varian) in transmission mode. TEM micrographs were obtained using an Hitachi 7000 transmission electron microscope operated at 100kV. Images were captured digitally using a Megaview 2 CCD camera. Specimens were prepared by dropping aqueous solutions of the NPs on to a formvar carbon-coated copper grid. Fluorescence measurements were performed on a Safire (Tecan) microplate reader. For NIR-664-N-succinimidyl ester-doped NPs, the excitation and emission wavelengths were set at 672 nm and 700 nm, respectively. Dynamic light-scattering (DLS) measurements were performed on a Zetasizer from Malvern instruments to yield values of the zeta potential (ζ) for the NPs.

Results and discussion

Optimisation of the dye-doping protocol

Several methods of doping the silica NPs with NIR dye were investigated. The major issue here was to prevent dye leaching. Non-porous silica NPs were prepared by lowering the pH below the isoelectric point of silica (pH ~2) [20]. However, at this low pH the dye is unstable and degrades to a non-fluorescent derivative. It was decided to use a higher pH and to conjugate the dye to an organosilane, aminopropyltriethoxysilane (APTES) prior to incorporation in the NP. This protocol produces NPs with a low residual porosity. APTES is a bifunctional ligand that contains both a dye-reactive amine group and a vitreophilic group. The amine group reacts with the succinimidyl ester group on the dye, via nucleophilic attack, to form a strong amide bond. The triethoxysilane group attaches to the growing silica NP via the sol-gel process. The conjugation was carried out in anhydrous *n*-hexanol. This is used as a co-surfactant in the microemulsion process and had no influence on the stability of the microemulsion. For example, using other solvents, for example dimethylformamide, led to NP aggregation and polydispersity. After centrifugation, the NPs were stored as a colloidal suspension in deionised water at 4 °C. Over a two-month period no measurable dye leaching was observed from the NPs.

Figure 3 shows the NP extinction spectra for different dye-loading values. On increasing amount of the dye, we observed a significant increase in the height of the peak at 620 nm relative to the peak at 670 nm. The peak at 670 nm corresponds to the free dye, whereas that at 650 nm relates to dimers. As the concentration is increased the peak broadens and shifts to a shorter wavelength, typical of the formation of more complex aggregates [21]. At 10% (*w*/*w*) most of the dye is in the aggregated form. In general, when cyanine dyes form complex aggregates, their fluorescence is quenched. The HFRET model has not been modified to account for this.

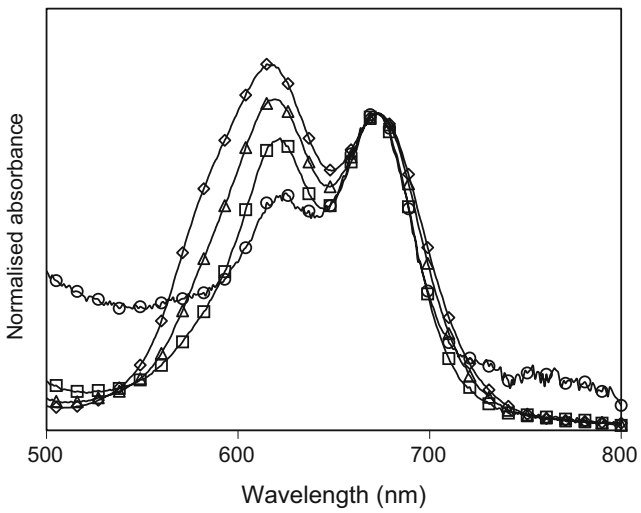

Fig. 3 UV-visible extinction spectra of silica NPs doped with NIR-664-succinimidyl ester at 1(*circles*), 3 (*squares*), 6 (*triangles*), 10 (*diamonds*) % (*w*/*w*) loading of dye

Table 1 The particle diameters, ∅ and ζ potentials for NPs prepared at different wt % of dye, measured using DLS

wt%	∅ (nm)	ζ(mV)
0.25	102+/−15	−37.8+/−8
0.5	103+/−20	−37.5+/−9
1	104+/−18	−35.5+/−6
2	105+/−19	−42.7+/−5
3	108+/−20	−42.3+/−9
6	110+/−18	−42.7+/−7
10	107+/−16	−39.4+/−8

Characterisation of NPs

The weight percent of dye, particle diameter, and ζ potentials measured using DLS for NPs functionalised with THPMP and APTMS are shown in Table 1. We used a combination of THPMP and APTMS to prevent NP aggregation and functionalise the surface for conjugation to biomolecules [19].

Only one peak was observed from DLS, indicating the NPs are monodispersed in size. Furthermore, the NPs did not aggregate over several months, because of the strongly negative zeta potentials. A TEM micrograph of the NPs is shown in Fig. 4. The average particle diameter was 68 ± 4.5 nm, which is significantly less than the value determined from DLS. This is because DLS measures the NP diameter plus the hydrodynamic ratio. The value of particle diameter determined from TEM was used below in the calculation of NP brightness ratio.

Measurement of NP quantum efficiency

We used a standard referencing method to calculate the quantum efficiency of the dye inside the NPs [22]. In this method, the ratio of the quantum efficiency of the dye inside the NPs, $\phi_{(\mathrm{dye,NP})}$ to the quantum efficiency of the free dye in solution, $\phi_{(\mathrm{dye,sol})}$, is determined using the following equation:

$$\frac{\phi(dye,NP)}{\phi(dye,sol)} = \left(\frac{F_{(dye,NP)}}{F_{(dye,sol)}}\right)_{c,k}$$

where $F_{(\mathrm{dye,NP})}$ is the fluorescence of the dye inside the NPs and $F_{(\mathrm{dye,\ sol})}$ is the fluorescence of the free dye in solution. The fluorescence is measured at the same dye concentration, c, and with the same instrument settings, k. The concentrations of the dye inside the NPs and in solution phase were determined using the Beer-Lambert law. In this calculation the extinction coefficient of the dye inside the NPs was assumed to be equal to that of the free dye in isopropanol, 187,000 L mol^{-1} cm^{-1}, at a wavelength of 672 nm.

In Fig. 5 we show the quantum efficiency as a function of NP dye loading. The black line corresponds to the quantum efficiency of free dye, previously determined to be 23% [15]. For loadings of less than 1% (*w*/*w*) we obtained a slight increase in the quantum efficiency to ~30%. At higher loading, the quantum efficiency dropped off due to HFRET and complex aggregation of the dye molecules [21].

Measurement of brightness ratio

The experimental brightness ratio of an NP over a single dye molecule was measured according to the method of Tan et al. [10]. First, the molar mass, M of the NPs is calculated using the following equation:

$$M = \frac{4}{3}\pi r^3 \rho N_A$$

where, r is the radius of the NP, determined from the TEM micrograph, ρ is the density of silica and N_A is Avogadro's

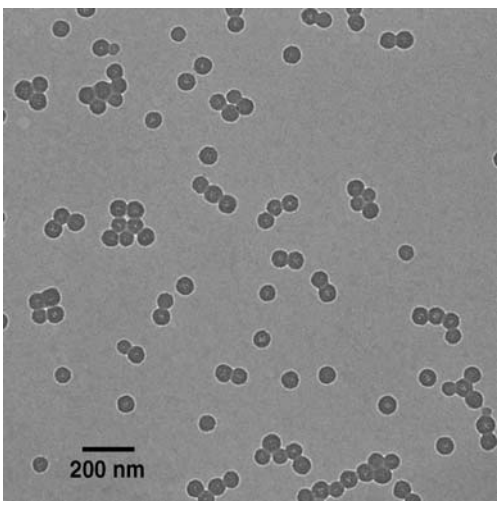

Fig. 4 TEM image of NIR dye-doped silica NPs

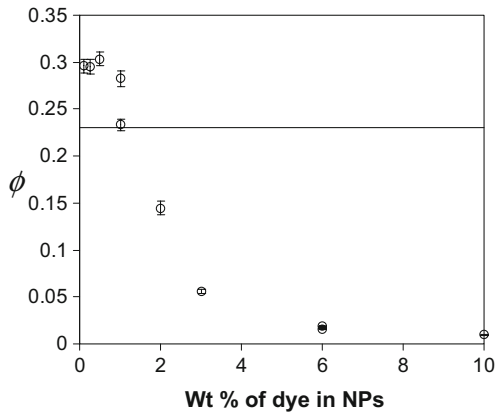

Fig. 5 Change in the quantum efficiency, ϕ of NIR-664-succinimidyl ester dye as the amount of dye is increased inside NPs. The *solid line* represents the quantum efficiency of the free dye

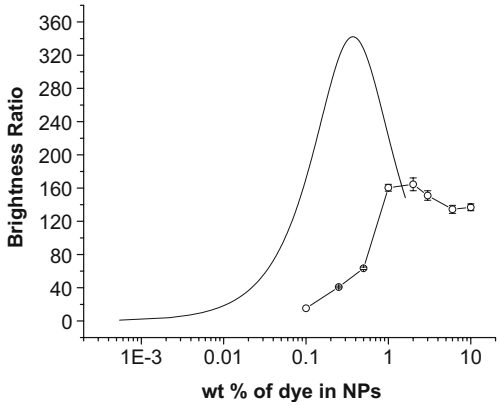

Fig. 6 The change in brightness ratio with increasing amount (% *w*/*w*) of NIR-664-succinimidyl ester dye inside NPs from experiment (*open circles*). The brightness ratio is the value of the fluorescence of the NPs divided by the fluorescence of free dye molecule at the same concentration. The results are compared with HFRET model results for a NP of radius 28 nm, with a Förster radius of 5.35 nm, and a quantum efficiency of 0.23

constant. In all fluorescence experiments we used a starting mass/volume concentration of 2 mg mL^{-1} of NPs in isopropanol. Using the above equation, this corresponds to a molar concentration of 4.3×10^{-9} mol L^{-1}. This is the concentration of fluorescent NPs in the colloidal suspension not the concentration of dye molecules. We measured the fluorescence of the NPs over a range of dilutions and compared the data with the fluorescence of pure dye of known concentration. All experiments were performed at the same instrument settings and constant temperature. The brightness ratio of the NPs, F_R was determined using the following equation:

$$F_R = \left(\frac{F_{NP}}{F_{dye}}\right)_c$$

where F_{NP} is the fluorescence of the NPs, and F_{dye} is the fluorescence of the dye at the same concentration. We also determined the brightness using Wiesner's method [23]. In this method the brightness ratio is calculated from the ratio of the quantum efficiencies of the dye inside the NP and pure dye multiplied by the number of dye molecules inside the NP. We obtained very similar values using the two methods. The brightness ratio of the NPs as a function of the dye loading in the NPs is shown in Fig. 6. This is directly compared with the brightness ratio, $F_{t,n}/F_o$ predicted from the HFRET model. We used a radius of 28 nm for the HFRET calculation which is equal to the radius of the NPs prior to functionalization with APTMS and THPMP. From experiment, at loadings of less than 1% (*w*/*w*) dye, we observed a steep increase in brightness with increasing dye load, in good agreement with theoretical predictions. A maximum value of brightness ratio was observed at 2% (*w*/*w*). However, there was very little difference between the fluorescence of NPs with 1 and 2% (*w*/*w*) dye loadings. This is higher than the optimum loading obtained from HFRET calculations, which was approximately 0.4% (*w*/*w*). This discrepancy is partly attributed to the fact that the experimental weight percent is calculated from the weight of dye added at the start of the experiment but the conjugation efficiency of the dye to amines is reported to be only ~70%. Hence the actual concentration would be lower. Moreover, the high pH used for catalysis of silica formation leads to aggregation of a small percentage of the dye. The combination of these effects means that the actual amount of dye inside the NPs is likely to be closer to the value predicted from the HFRET calculation.

For the NPs, the maximum brightness ratio measured experimentally was 165 at 2% (*w*/*w*) (Fig. 6). This is approximately 50% less than the value of 342 which was predicted from the HFRET calculation. Although the HFRET model does overestimate the brightness ratio it does provide a simple method for screening near-infrared dyes as candidates for high brightness NPs.

In previous work, using $Ru(bpy)_3Cl_2$ a loading of 21% (*w*/*w*) was achieved without a drop in fluorescence [10]. This is attributed to the large Stokes shift of 157 nm for the ruthenium complex, compared with the 22 nm Stokes shift for the NIR-664 dye used in this study. Therefore, the energy losses due to energy transfer are much less significant for the ruthenium complex-doped NPs. However, dyes that fluoresce at shorter wavelengths are less desirable for biomedical diagnostics for the reason discussed previously.

Conclusion

We have prepared high-brightness NPs doped with an inexpensive, Cy5-surrogate NIR dye. An optimum brightness ratio for the NPs corresponded to a dye loading of approximately 2% (*w*/*w*). At this loading the NPs were significantly brighter than free dye molecules. The HFRET effect, which occurs when dye molecules with small Stokes shift are in close proximity, was modelled for our system and good agreement was obtained between experimental results and model predictions. Furthermore, the model can be used as a predictive tool for screening dyes for use in high-brightness NPs. The results reported in this work point the way to a strategy for enhancing the brightness ratio and, subsequently, improved sensitivity and LOD in fluorescence biosensing. In future work we intend to investigate the benefits of NIR dye-doped NPs in biosensing, particularly fluoro-immunoassays.

Acknowledgment This material is based upon work supported by the Science Foundation Ireland under Grant No. 05/CE3/B754.

References

1. Haugland RP (2005) The handbook—a guide to fluorescent probes and labelling technologies. Molecular Probes, Eugene
2. Burns A, Ow H, Wiesner U (2006) Chem Soc Rev 35:1028–1042
3. Wang F, Tan W, Zhang Y, Fan X, Wang M (2006) Nanotechnology 17:R1–R13
4. Medintz I, Uyeda H, Goldman E, Mattoussi H (2005) Nature Mater 4:435–446
5. Chan WCW, Nie SM (1998) Science 285:2016–2018
6. Stöber W, Fink A, Bohn E (1968) J Colloid Interface Sci 26:62–69
7. Ow H, Larson D, Srivastava M, Baird B, Webb W, Wiesner U (2005) Nano Lett 5:113–117
8. Osseo-Asare K, Arriagada FJ (1990) Colloids Surf 50:321–339
9. Santra S, Zhang P, Wang K, Tapec R, Tan W (2001) Anal Chem 73:4988–4993
10. Lian W, Litherland SA, Badrane H, Tan W, Wu D, Baker HV, Gulig PA, Lim DV, Jin S (2004) Anal Biochem 334:135–144
11. Hoon KS, Jeyakumar M, Katzenellenbogen JA (2007) J Am Chem Soc 129:13254–13264
12. Wang L, Tan W (2006) Nano Lett 6:84–88
13. Wang L, Zhao W, O'Donoghue MB, Tan W (2007) Bioconj Chem 18:297–301
14. Deng T, Li J-S, Jiang J-H, Shen G-L, Yu R-Q (2006) Adv Funct Mater 16:2147–2155
15. Mank AJG, Yeung ES (1995) J. Chromatogr A 708:309–321
16. Novotny L, Hecht B (2007) Principles of nano-optics. Cambridge University Press, UK
17. Lakowicz JR (1999) Principles of fluorescence spectroscopy. Kluwer Academic Press, New York
18. Yao G, Wang L, Wu Y, Smith J, Xu J, Zhao W, Lee E, Tan W (2006) Anal Bioanal Chem 385:518–524
19. Bagwe RP, Hilliard LR, Tan W (2006) Langmuir 22:4357–4362
20. Zhao X, Bagwe RP, Tan W (2004) Adv Mater 16:173–176
21. West W, Pearce S (1965) J Phys Chem 69:1894–1903
22. Williams ATR, Winfield SA, Miller JN (1983) Analyst 108:1067–1071
23. Larsons DR, Ow H, Vishwasrao HD, Heikal AA, Wiesner U, Webb WW (2008) Chem Mater 20:2677–2684